# Measurements of the Fracture Energy of Lithiated Silicon Electrodes of Li-Ion Batteries

Matt Pharr, Zhigang Suo, and Joost J. Vlassak*

School of Engineering and Applied Sciences, Harvard University, Cambridge, Massachusetts 02138, United States

ABSTRACT: We have measured the fracture energy of lithiated silicon thin-film electrodes as a function of lithium concentration. To this end, we have constructed an electrochemical cell capable of testing multiple thin-film electrodes in parallel. The stress in the electrodes is measured during electrochemical cycling by the substrate curvature technique. The electrodes are disconnected one by one after delithiating to various states of charge, that is, to various concentrations of lithium. The electrodes are then examined by optical microscopy to determine when cracks first form. All of the observed cracks appear brittle in nature. By determining the condition for crack initiation, the fracture energy is calculated using an analysis from fracture mechanics. In the same set of experiments, the fracture energy at a second state of charge (at small concentrations of lithium) is measured by determining the maximum value of the stress during delithiation. The fracture energy was determined to be $\Gamma = 8.5 \pm 4.3$ J/m^2 at small concentrations of lithium ($\sim$Li$_{0.7}$Si) and have bounds of $\Gamma = 5.4 \pm 2.2$ J/m^2 to $\Gamma = 6.9 \pm 1.9$ J/m^2 at larger concentrations of lithium ($\sim$Li$_{2.8}$Si). These values indicate that the fracture energy of lithiated silicon is similar to that of pure silicon and is essentially independent of the concentration of lithium. Thus, lithiated silicon demonstrates a unique ability to flow plastically and fracture in a brittle manner.

KEYWORDS: Lithium-ion batteries, silicon, fracture energy, fracture toughness
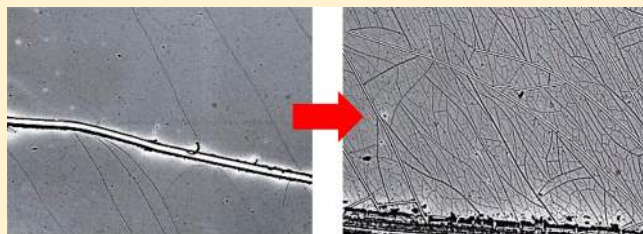
Lithium-ion batteries provide the power for most portable electronics and have found applications in electric vehicles.[1,2] Recent research in the area has focused on designing batteries with high energy density, long cycle life, low cost, and safe operation.[3,4] In fulfilling these requirements, silicon has been identified as a promising material for anodes, as it can host a very large amount of lithium.[5] Lithiation of silicon results in a volumetric expansion of approximately 300%, which, under constraint, can result in very large mechanical stresses and fracture.[6] Fracture of the electrode leads to loss of active material and results in more surface area for solid electrolyte interphase (SEI) growth; both factors substantially contribute to capacity fade of the system.[6–8]

A number of recent experimental studies have measured mechanical properties of silicon electrodes. For instance, Sethuraman et al. used the substrate curvature method to measure the stress in thin-film silicon electrodes as a function of lithium concentration. They found that lithiated silicon flows plastically at a stress of $\sim$1.7 GPa for Li$_{0.3}$Si, with this stress decreasing to $\sim$1 GPa for Li$_2$Si.[9] Soni et al. and Zhao et al. performed similar measurements and have found comparable results.[10,11] Hertzberg et al. used nanoindentation methods to measure the hardness and elastic modulus of lithiated nanocrystalline thin-film silicon electrodes as a function of lithium concentration. They found that the hardness decreases from 5 to 1.5 GPa and the elastic modulus decreases from 92 to 12 GPa in transitioning from the pure nanocrystalline silicon phase to the fully lithiated phase (Li$_{15}$Si$_4$).[12] Sethuraman et al. measured the biaxial elastic modulus of thin-film silicon

electrodes as a function of lithium concentration using the substrate curvature method, finding a biaxial modulus of 70 GPa for Li$_{0.32}$Si and 35 GPa for Li$_3$Si.[13] Kushima et al. measured the tensile strength of single-crystal silicon nanowires, finding a strength of 3.6 GPa for unlithiated silicon nanowires and a strength of 0.72 GPa for lithiated silicon nanowires (Li$_{15}$Si$_4$).[14] In addition to these experimental studies, a number of theoretical works have examined the fracture of silicon electrodes.[15–24] An important parameter in these analyses is the fracture energy of the lithiated phase. Thus far, in these theoretical works, the values of the fracture energy are merely educated guesses since no quantitative measurements have been performed. Moreover, a single number is usually assigned, despite the possibility of the fracture energy varying with lithium concentration.

In this Letter, we devise a method to measure the fracture energy of lithiated silicon thin-film electrodes. To achieve this goal, we have constructed an electrochemical cell with an array of parallel electrodes allowing us to lithiate/delithiate the electrodes to different states of charge, while performing in situ stress measurements. The electrodes were then examined by microscopy both to observe the morphological development of the cracks and to construct a bound on the critical state of charge corresponding to the formation of cracks. By

determining this critical state of charge and knowing the corresponding state of stress, we quantify the fracture energy through an analysis from fracture mechanics. From the same set of experiments, we can obtain an additional measurement of the fracture energy at a second state of charge—at small concentrations of lithium—by determining the maximum value of the substrate curvature during delithiation.

Silicon electrodes typically have features on the order of 100 nm and include nanowires,[25,26] nanoporous structures,[27] nanoparticles,[28,29] and thin-films.[10,21,30−32] Of these options, quantitative electrochemical characterization of individual nanowires and nanoparticles proves prohibitively difficult. Thus, in this study, thin films were selected as the working electrodes. Glass substrates with a thickness of 1 mm were cleaned with acetone and isopropanol and placed into a sputter deposition system (AJA Int. ATC 1800) with a base pressure of <10^−8 Torr. All sputtering targets had a 50.8 mm diameter, and depositions were performed at room temperature (22 °C). First, the samples were plasma-cleaned in Ar at 20 mTorr and an RF power of 24 W for 5 min. Next, 15 nm of Ti was sputtered onto the substrates using a pressure of 3 mTorr of Ar and a DC power of 100 W for 5 min. A 300 nm layer of Cu was then deposited on the Ti underlayer using a pressure of 5 mTorr of Ar and a DC power of 100 W for 15 min. The Cu film serves as current collector, while the Ti underlayer is used to improve the adhesion between the Cu film and the glass substrate. Finally, a 300 nm Si film was deposited on the Cu current collector using a pressure of 5 mTorr of Ar and a DC power of 100 W for 78 min. The working area of each silicon electrode was 8 mm × 20 mm. After deposition, X-ray diffraction was used to verify the amorphous structure of the sputtered Si thin-films.

Electrochemical experiments were conducted in a custom-fabricated hermetic Teflon electrochemical cell with a glass window (Figure 1). The cell employs a Li reference electrode, seven Si working electrodes, and seven Li counter electrodes. In essence, it is a three-electrode configuration but with multiple working and counter electrodes operating in parallel. A schematic of the cell is shown in Figure 1; only three working and reference electrodes are shown for simplicity, whereas seven of each are actually used in the experiments. This arrangement resulted in a total resistance from the galvanostat to the electrodes (including contact resistance with the electrode) of less than 2Ω for each connection, which resulted in a voltage drop of less than 400 μV in these experiments. The cell was assembled in a glovebox maintained at <0.1 ppm moisture and used a 1 M solution of $LiPF_6$ in 1:1:1 (weight %) ethylene carbonate−diethyl carbonate−dimethyl carbonate as the electrolyte. Electrochemical measurements were performed with a VersaSTAT 3 galvanostat from Princeton Applied Research. The seven silicon electrodes were lithiated simultaneously at a constant current density of 15 μA/cm² (a C/16 rate assuming a capacity of 3579 mAh/g) to a cutoff potential of 0.01 V. Although not pursued in this study, this cutoff potential in principle can be varied to examine properties as a function of lithium concentration. The relatively slow rate of lithiation was selected to allow enough time for diffusive equilibrium through the films.[10,33] The electrodes were then delithiated at the same current density (15 μA/cm²). At various stages of delithiation (as marked by red arrows in Figure 2), the electrodes were disconnected one by one from the cell such that they were only partially delithiated. Delithiation then resumed with a new current such that the current density
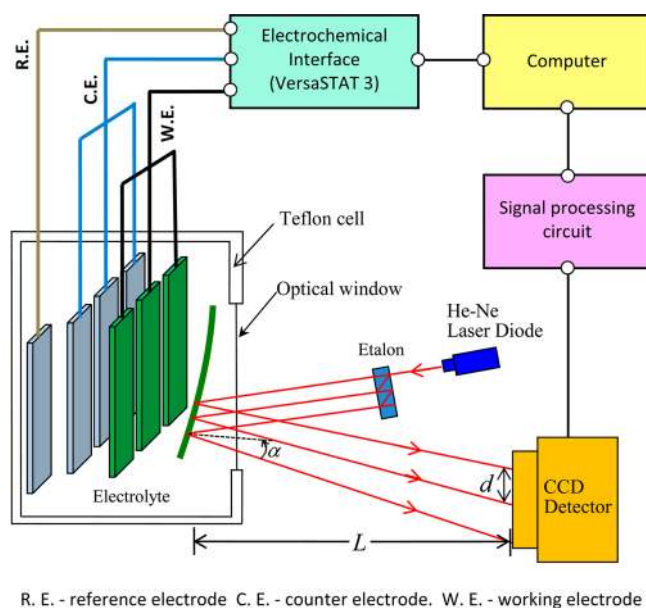

Figure 1. A schematic representation of the custom-made electrochemical cell with in situ multibeam optical sensor. Only three working electrodes and counter electrodes are drawn; there are seven working electrodes and counter electrodes in the actual cell. The stress is measured in one of the working electrodes, as depicted by the rightmost green line, which shows the electrode after bending due to lithium insertion.

remained constant during the entire delithiation sequence. One electrode in each test was fully delithiated to a cutoff potential of 2 V.

For the electrode that was fully delithiated, the stress in the film was measured by monitoring the substrate curvature in situ during lithiation/delithiation. The average stress in the film was deduced from the curvature of the substrate using Stoney's equation:[34,35]

$$\sigma = \sigma_r + \frac{E_s h_s^2}{6 h_f (1 - \nu_s)} \Delta K \tag{1}$$

where σ is the average stress in the film, E_s is the elastic modulus of the substrate, h_s is the thickness of the substrate, h_f is the thickness of the film, ν_s is Poisson's ratio of the substrate, and ΔK is the change in curvature of the substrate that results from the stress in the film. σ_r denotes the initial residual stress in the film, that is, the stress that developed during sputter deposition. This stress was determined by measuring the curvature of the substrate before and after silicon deposition. It is important to note that knowledge of the properties of the film other than the thickness is not required to evaluate the stress using Stoney's equation. In the calculations, values of E_s = 77 GPa and ν_s = 0.22 were used for the glass substrates.

We should also note that SEI growth during the initial lithiation may contribute to the measured stress. To address this point, we have performed additional experiments (not included here) on electrodes with identical surface areas but with different initial film thicknesses of 100 and 300 nm. Due to the smaller film thickness, the SEI will have a larger relative contribution to the measured stresses in the 100 nm film. However, the stresses (not accounting for SEI formation) that we measure in the two experiments are almost identical. Hence, it appears that the stresses we measure in our experiments are primarily due to those that develop in the silicon film, and we
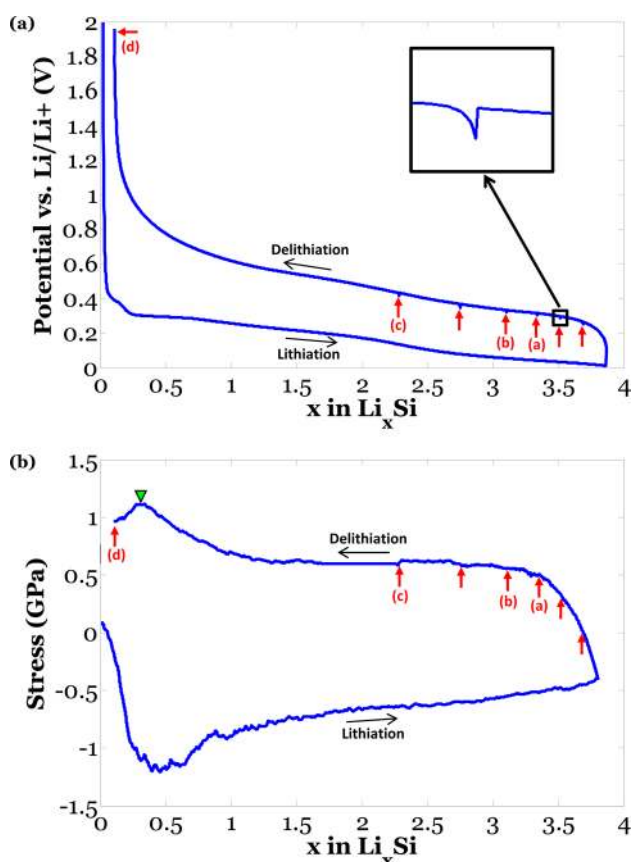
Figure 2. Representative responses in (a) potential vs Li/Li+ and (b) stress as a function of lithium concentration from a galvanostatic test of a set of seven 300 nm a-Si thin films. During delithiation, the electrodes are disconnected at various concentrations of lithium, as indicated by the red arrows. The inset in a shows a zoomed-in view near one of these points. The letters near some of the arrows correspond to the images labeled in Figure 3. The green triangle in b indicates the location of the maximum tensile stress.

have thus neglected any contribution of the SEI to the measured stress.

The volume of the film, V_f, is taken to be linear in the state of charge,

$$V_f = V_f^0(1 + \beta s) \qquad (2)$$

where V_f^0 is the initial volume of the film, β is related to the atomic volumes (Ω) by $\beta = (\Omega_{Li3.75Si} - \Omega_{Si})/\Omega_{Si}$, and s is the state of charge of the silicon electrode, with a value of 0 representing pure silicon and a value of 1 representing the fully lithiated state (assumed to be $Li_{3.75}Si$ with a capacity of 3579 mAh/g).[36] According to Obrovac et al., Si will undergo a 280% increase in volume upon reaching the fully lithiated state of $Li_{3.75}Si$, that is, $\beta = 2.8$.[36] Using atomic force microscopy, He et al. and Beaulieu et al. measured similar values in patterned amorphous silicon films.[37,38] Moreover, both groups found that the volume increased linearly with lithium concentration.[37,38] For a thin-film geometry, lithium insertion is accommodated entirely by growth in the thickness direction due to the constraint in the in-plane directions placed by the relatively thick substrate. Thus, the thickness of the film, h_f, takes the same form as in eq 2:

$$h_f = h_f^0(1 + \beta s) \qquad (3)$$

where h_f^0 is the initial thickness of the film. The initial thicknesses of the Si electrodes were measured by profilometry and were approximately 300 nm (± 15 nm) for all of the sputtered films.

The curvature of the substrate was monitored with a multibeam optical sensor (MOS) from k-space associates (Figure 1). The MOS employs an array of parallel laser beams to measure the curvature of the substrate. The array of laser beams allows simultaneous illumination and detection, which in turn greatly reduces noise in the measurements caused by fluid motion in the electrochemical cell or by ambient vibrations. The cell is also placed on an antivibration table during testing. The change in the curvature of the substrate (see Figure 1) is calculated from the geometric relation

$$\Delta K = \frac{d_0 - d}{d_0}\left[\frac{\cos \alpha}{2L}\right]\frac{n_a}{n_e} \qquad (4)$$

where d is the distance between two adjacent laser spots measured on the CCD camera, d_o is the initial distance between the laser spots, α is the angle of reflection of the laser beams, L is the distance between the electrochemical cell and the CCD camera, and n_a and n_e are the indices of refraction of air and the electrolyte, respectively. Since the laser passes through air, the electrolyte, and an optical window, refraction of the laser beams at these corresponding interfaces must be taken into account, which is the source of the quantity n_a/n_e. In the calculation of the stress, we took $n_e = 1.42$ for the electrolyte[39] and $n_a = 1$ for air. Neglecting refraction of the laser beams would result in a substantial error in the curvature measurement of approximately 40%.

The biaxial elastic modulus of the lithiated silicon is determined by measuring the stresses during the initial stage of delithiation. In this stage, the in-plane strain associated with lithium extraction from the electrode is accommodated entirely by elastic deformation. At a particular state of charge, s, the volume of the electrode is given by eq 2. At a state of charge, $s + \Delta s$, where Δs is sufficiently small to ensure elastic deformation of the film, the volume of the film is $V_f = V_f^0[1 + \beta(s + \Delta s)]$, and thus the volumetric strain is $[V_f(s + \Delta s) - V_f(s)]/V(s) = \beta\Delta s/(1 + \beta s)$. Hence, in going from a state of charge, s, to a state of charge, $s + \Delta s$, the increment in the linear strain induced by lithiation, $\Delta\varepsilon^l$, is

$$\Delta\varepsilon^l = \frac{1}{3}\frac{\beta\Delta s}{1 + \beta s} \qquad (5)$$

Due to the constraint placed by the substrate, the total in-plane strain vanishes, and the lithiation strain necessarily results in an elastic strain $\Delta\varepsilon^e = -\Delta\varepsilon^l$, which in turn results in a stress given by Hooke's law. For a thin film, the stress state is equal biaxial, and the increment in the stress $\Delta\sigma$ is

$$\Delta\sigma = \frac{E_f}{1 - \nu_f}\Delta\varepsilon^e \qquad (6)$$

where ν_f is Poisson's ratio of the film and E_f is the elastic modulus of the film. Thus,

$$\frac{E_f}{1 - \nu_f} = -3\frac{1 + \beta s}{\beta}\frac{\Delta\sigma}{\Delta s} \qquad (7)$$

Using eq 7, one can calculate the biaxial modulus of the film, $E_f/(1 - \nu_f)$, by measuring the state of charge and stress during the elastic stage of delithiation.
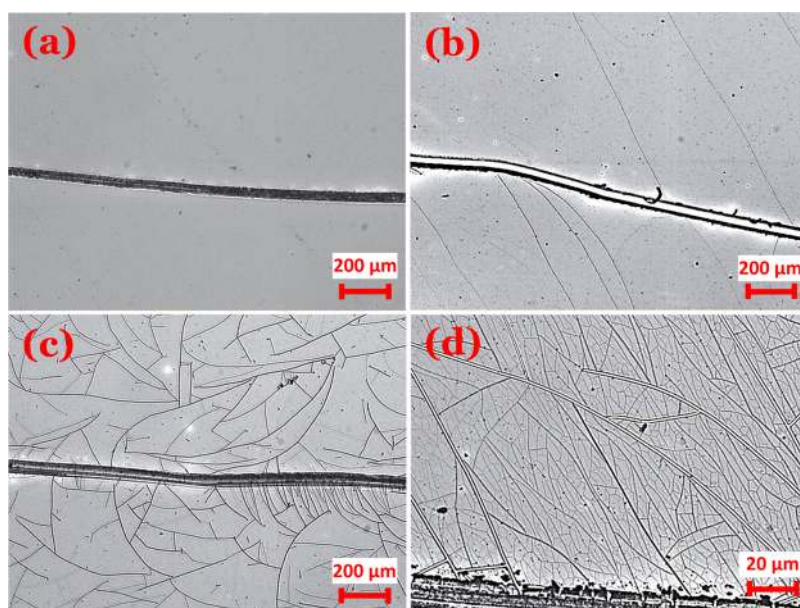
Figure 3. Optical micrographs of the electrodes tested in Figure 2. The labels a−d correspond to the point at which the electrode was disconnected from the cell, as indicated in Figure 2.

To image the electrodes, they were removed from the cell in the glovebox, rinsed in dimethyl carbonate, and dried. Next, they were immersed in mineral oil and covered with a glass slide to prevent any exposure of lithiated silicon to air. The samples were then removed from the glovebox and examined using an optical microscope. This technique allowed us both to construct a bound on when cracks initially form and to examine the evolution of the crack morphology with further delithiation. The same goal could be achieved by direct monitoring of the surface of a single electrode during delithiation, but simultaneous integration of optical microscopy and stress measurements with the electrochemical cell is not straightforward. For observation in the scanning electron microscope (SEM), the samples were sealed in an airtight container in the glovebox and immediately transferred to the SEM chamber. It was estimated that the samples were exposed to air for less than two minutes during transfer to the SEM.

Figure 2 shows a typical response of the potential and stress measured during lithiation/delithiation. During delithiation, the electrodes are removed one by one at the points represented by red arrows in Figure 2. In Figure 2a, we can see that the voltage gradually decreases with the state of charge. This voltage profile can be contrasted with the extremely flat voltage profiles observed during the initial lithiation of crystalline silicon wafers.[40,41] Such flat profiles indicate a two-phase reaction in crystalline silicon, while the sloping profiles observed here indicate a single-phase reaction. Recently, McDowell et al. and Wang et al. have performed in situ transmission electron microscopy (TEM) observations during the initial lithiation of individual amorphous silicon nanoparticles.[42,43] Both groups have identified a phase front separating amorphous silicon from amorphous lithiated silicon, that is, the initial lithiation of amorphous silicon occurred by a two-phase mechanism in their experiments.[42,43] We propose that the lithiation rate is the critical difference between our experiments and those performed on the individual amorphous nanoparticles. In the latter, full lithiation occurs in approximately 100 s, whereas in our work, full lithiation occurs over 16 h. The relatively slow

rates used in our experiments apparently engender lithiation through a single-phase reaction mechanism.

A typical sequence of the measured stress is shown in Figure 2b. The film initially is under residual tension (70 MPa in this case), which results from the sputtering process. The stress becomes more and more compressive as lithium is inserted into the electrode until it begins to flow plastically at a stress of −1.2 GPa and a concentration of $Li_{0.4}Si$. Upon further lithiation, the film continues to flow plastically with a continuous small reduction in the stress, reaching a value of −450 MPa at the fully lithiated concentration of $Li_{3.75}Si$. We note that these values compare quite well to the hardness values reported by Hertzberg et al.[12] In particular, using the relation $\sigma_Y = H/3$, where H is the indentation hardness, Hertzberg et al. found values of $\sigma_Y = 1.1$ GPa for $Li_{0.6}Si$ and $\sigma_Y = 550$ MPa for $Li_{3.75}Si$.[12] During delithiation, the stress becomes more and more tensile until it begins to flow in tension at a stress of 500 MPa and a concentration of $Li_{3.4}Si$. Additional delithiation results in further plastic flow with a continuous increase in stress, reaching a maximum value of 1.12 GPa at a lithium concentration of $Li_{0.33}Si$. After this point, the measured value of the stress decreases with further delithiation.

We should also point out that, in Figure 2, the horizontal axes are constructed by integrating the current during the experiment to get the total charge. However, the amount of charge does not necessarily represent the concentration of lithium in silicon, as SEI formation may consume some lithium. Recently, Nadimpalli et al. quantified the capacity loss due to SEI formation.[8] In their experiments, they used the same electrodes, the same electrolyte, and very similar electrochemical loading conditions as in our experiments. They have found that the charge lost per surface had an upper bound of 0.023 mAh/cm^2.[8] This loss corresponds to a capacity of 329 mAh/g in our experiments, which is less than 10% of the total capacity (3579 mAh/g). Thus, there may be a systematic error of at most 10% in the values of the lithium concentration reported in Figure 2.

Figure 3 shows optical micrographs of the electrodes at various extents of delithiation. The images in this figure were

D

taken at locations near scratches in the film introduced by a diamond scribe. The labels a−d in Figure 3 correspond to the labeled red arrows shown in Figure 2, indicating the extent to which each of the electrodes was delithiated. The electrode in Figure 3a shows no evidence of fracture, whereas the electrode in Figure 3b does. From this observation, we can quantify a bound on the fracture energy by calculating the range of energy release rates between these two lithium concentrations (i.e., between the points labeled a and b in Figure 2b). Upon further delithiation, more cracks are formed, and the electrode develops a distribution of crack widths as illustrated in Figures 3d and 4a. The very wide cracks (Figure 4b) are formed during
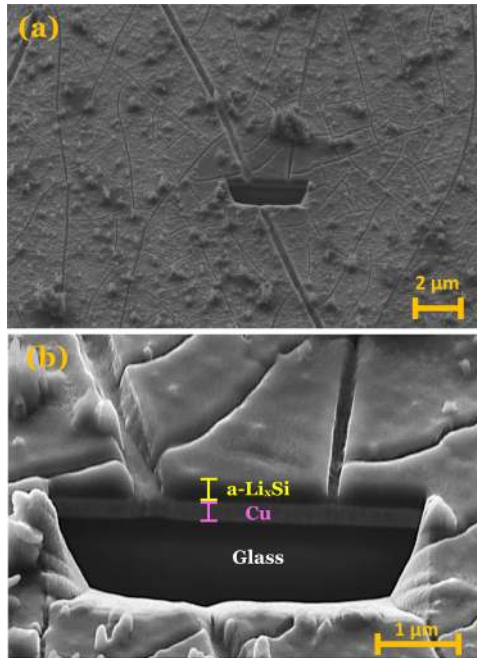

Figure 4. SEM images near a FIB cross-section of a 300 nm a-Si electrode after one cycle at (a) 10 000× magnification and (b) 50 000× magnification.

the earlier stages of delithiation (such as those seen in Figure 3b) and widen with subsequent delithiation. This process is most likely caused by an interfacial sliding mechanism as discussed in a number of previous works.[20,21] The narrower cracks (the majority of the cracks as seen in Figures 3d and 4a) are formed between the points indicated by arrows c and d in Figure 2, which allows us to calculate a value of the fracture energy at low concentrations of lithium (discussion to follow).

To calculate these energy release rates, one has to be particularly careful due to the flow of the lithiated silicon during the experiments and the possibility of sliding at the interface between the lithiated silicon and copper. If the initial flaw size is small compared to the thickness of the film, the energy release rate, G, takes the form:

$$G = Z \frac{\sigma^2 a}{\overline{E}_f} \tag{8}$$

where Z is a nondimensional parameter and a is the length of the initial flaw. For instance, for a crack of length $2a$ in an infinite body, $Z = \pi$.[44] For a thin-film geometry, Nakamura and Kamath investigated the energy release rate as a function, a/h: the ratio of crack length to film thickness.[45] For $a/h \ll 1$, the

analysis given by eq 8 is appropriate. For $a/h \geq 1$, Nakamura and Kamath show that the energy release rate becomes independent of the flaw size such that a steady-state analysis performed by Beuth is appropriate.[45] Beuth's analysis is for a steady-state channeling crack in an elastic thin film bonded to an elastic substrate.[46] The energy release rate is given by

$$G = g(\alpha, \beta) \frac{\sigma^2 h_f}{\overline{E}_f} \tag{9}$$

where $\overline{E}_f = E_f/(1 - \nu_f^2)$ is the plane-strain modulus of the film, and $g(\alpha,\beta)$ is a function of the Dundurs parameters, α and β, which are defined by

$$\alpha = \frac{\overline{E}_f - \overline{E}_s}{\overline{E}_f + \overline{E}_s}, \qquad \beta = \frac{\mu_f(1 - 2\nu_s) - \mu_s(1 - 2\nu_f)}{2\mu_f(1 - \nu_s) + 2\mu_s(1 - \nu_f)} \tag{10}$$

where the $\overline{E}_i = E_i/(1 - \nu_i^2)$ represent the respective plane-strain moduli, and the $\mu_i = E_i/[2(1 + \nu_i)]$ represent the respective shear moduli.[46]

The analysis by Beuth does not take into account the effects of interfacial sliding, a phenomenon suggested to occur at the lithiated silicon/copper interface in a number of studies.[20,21,32] By allowing for interfacial sliding and using a shear lag approximation, Hu and Evans found that the energy release rate in the steady state takes the form

$$G = \left[\frac{\sigma}{3\tau_0} + F(\Sigma) \right] \frac{\sigma^2 h_f}{E_f} \tag{11}$$

where τ_o is the interfacial sliding strength, $\Sigma = E_f/E_s$, and $F(\Sigma)$ is a function of the elastic mismatch between the film and the substrate, which is analogous to the function $g(\alpha,\beta)$ given in eq 9.

To determine the form of the energy release rate applicable to our experiments, we must first consider the initial flaw size in our experiments. Unfortunately, we do not know the characteristic flaw size created during sputter deposition, and hence it is not possible to use eq 8 directly. To circumvent this issue, each of the thin-film silicon electrodes was scratched with a diamond scribe to introduce imperfections with sizes on the order of the film thickness so that the analysis by Beuth is appropriate.[45] By comparison, the steady state implied in eq 11 is reached only when the crack length approaches the characteristic size of the sliding zone, $l_p = \sigma h/\tau_o$. Using a representative value of $\tau_o = 40$ MPa,[20] $l_p \approx 10$ μm in our experiments. Thus, the energy release rate does not approach the expression given in eq 11 until the crack length is much larger than the initial flaw size. Also, the first term in brackets in eq 11 represents the contribution of interfacial sliding. Thus, interfacial sliding only increases the crack driving force as compared to the analysis of Beuth,[46] that is, the more "difficult" step in the crack propagation process in our experiments is that associated with eq 9.

Using the appropriate expression for the energy release rate (eq 9), we can calculate a bound on the fracture energy of heavily lithiated silicon. Fracture initiates when the energy release rate reaches the fracture energy of the material, $G = \Gamma$, which is bounded by the points corresponding to Figure 3a and b. For the fracture energy measurements at these large concentrations of lithium, we have used the values of E_f measured from initial delithiation (Table 1), where a value of $\nu_f = 0.26$ has been assumed.[33] The value of the function $g(\alpha,\beta)$

Table 1. Results of Four Experiments To Determine the Fracture Energy of Lithiated Silicon at Large Concentrations of Lithium[a]

test no.	x in Li$_x$Si	E (GPa)	Γ (J/m^2)
1	3.0−3.2	46.1	7.6−9.4
2	2.8−3.0	23.0	2.4−5.6
3	2.4−2.6	29.4	6.5−7.5
4	2.4−2.7	33.0	5.0−5.2

[a]The second column represents the range in concentration over which fracture first occurred. The third column is the elastic modulus calculated from initial delithiation of the electrodes. The final column is the calculated range of fracture energies corresponding to the concentration range in the second column.

was determined by interpolating the values reported by Beuth[46] and was approximately 1.5 in all experiments. The results from four separate experiments are shown in Table 1. The quantity x in the table represents the range of lithium concentrations over which fracture initially occurred in each test. The mean and standard deviation were found to be E_f = 32.9 ± 9.7 GPa for the modulus and Γ = 5.4 ± 2.2 J/m^2 to Γ = 6.9 ± 1.9 J/m^2 for the lower and upper bounds on the fracture energy.

We have also monitored the morphological development of the cracks in the electrodes (Figure 3). Cracks initially form with spacings that are much larger than the thickness of the film (Figures 3b,c). At later stages of delithiation, many more cracks are formed, and the crack spacing approaches the thickness of the film (Figures 3d and 4). Beuth[46] calculated the change in curvature of the substrate, δK, due to cracks with a characteristic spacing, p, and found

$$\delta K = -\frac{12(1 - \nu_s)\sigma h_f^2}{E_s h_s^2 p}g(\alpha, \beta) \tag{12}$$

Dividing eq 12 by the curvature calculated from Stoney's equation (assuming zero curvature for zero stress) gives the relative contribution of the cracks to the curvature:

$$\frac{\delta K}{K} = -2g(\alpha, \beta)\frac{h_f}{p} \tag{13}$$

From eq 13 it is evident that cracks tend to decrease the curvature (we have taken a positive sign as indicating the curvature created by tension in the film). Also, the contribution from the cracks is insignificant until the crack spacing approaches a few times the thickness of the film. We note that the analysis presented in eqs 12−13 does not include the effects of sliding. However, such effects will not be significant until the crack spacing approaches the length of the sliding zone, $l_p = \sigma h/\tau_o$, which is approximately 10 μm for our experiments.[20] The crack spacings shown in Figure 3c are on the order of hundreds of micrometers, much larger than the representative length of the sliding zone. Thus, we believe that cracks such as those in Figure 3c still do not significantly affect the curvature of the substrate. Instead, only the cracks formed at the latest stages of delithiation (Figures 3d and 4), with spacings on the order of 1−2 μm, affect the stress measured from the substrate curvature technique. As a result, one can identify the lithium concentration at which extensive additional cracking occurs by locating the point at which the apparent tensile stress starts to decrease, that is, the concentration marked by the green arrow in Figure 2b. From this point, we gain an additional measurement of the fracture energy of

lithiated silicon at small concentrations of lithium from the same test. The results of these measurements are shown in Table 2 for the same four tests that were listed in Table 1. In

Table 2. Results of Four Experiments To Determine the Fracture Energy of Lithiated Silicon at Small Concentrations of Lithium[a]

test no.	x in Li$_x$Si	E (GPa)	Γ (J/m^2)
1	0.33	50	14.9
2	0.73	30	6.6
3	0.86	34	7.0
4	1.01	36	5.4

[a]The second column lists the lithium concentrations corresponding to the maximum tensile stress (green arrow in Figure 2b). The third column is the elastic modulus taken from ref 13. The final column contains the fracture energies calculated corresponding to the maximum tensile stress.

these calculations, the values for the elastic moduli are taken from ref 13 since we did not measure the moduli at these concentrations in our experiments.[13] The quantity x in Li$_x$Si in Table 2 represents the lithium concentration corresponding to the maximum curvature. Using this technique, the mean value of the fracture energy at this lower concentration of lithium is Γ = 8.5 ± 4.3 J/m^2.

In addition to these experiments, we performed a few tests on individual silicon electrodes in a standard three-electrode arrangement. The results of three such tests are shown in Figure 5. These tests were performed at the same conditions as
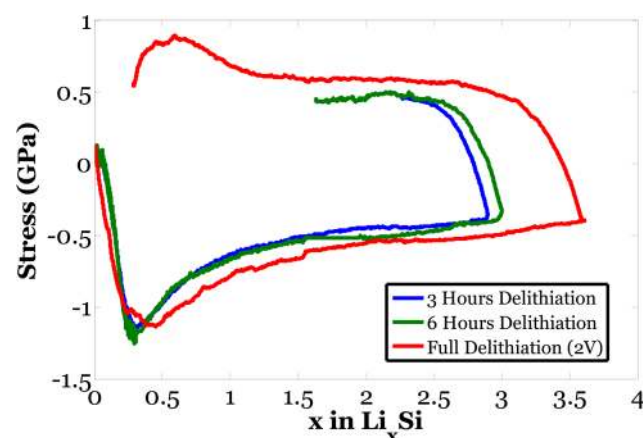

Figure 5. Responses in stress as a function of lithium concentration from galvanostatic tests of individual 325 nm silicon electrodes. The electrodes corresponding to each test are delithiated to different extents to determine the fracture energy.

previously discussed. In particular, the electrodes were lithiated galvanostatically at a current density of 15 μA/cm^2 to a cutoff potential of 0.01 V. The three tests vary in the extent to which they are allowed to delithiate. In the first test, the electrode is delithiated for three hours, and no fracture is observed (similar to Figure 3a). In the second test, the electrode is delithiated for six hours, and some fracture is seen (similar to Figure 3b). In the third test, the electrode is fully delithiated to a cutoff potential of 2 V, and extensive fracture is seen (similar to Figure 3d). Following the previously discussed procedure, we can quantify the fracture energy. This set of experiments yields a bound on the fracture energy of Γ = 7.5−8.7 J/m^2 in the

concentration range of $Li_{1.6}Si-Li_{2.3}Si$ and a fracture energy of $\Gamma = 14.7 \text{ J/m}^2$ for $Li_{0.6}Si$. Although on the higher end of the spectrum, these values fall within the range of values shown in Tables 1 and 2 for the experiments performed on multiple electrodes.

It is important to note that eq 9 invokes an analysis from elasticity, while Figure 2b suggests that lithiated silicon is capable of plastic flow. The applicability of linear elastic fracture mechanics to lithiated silicon is an open question. According to the theory established for metals, linear elastic fracture mechanics is applicable when the plastic zone at the front of the crack is much smaller than the feature size of the specimen.[47] The plastic zone size is estimated by[47]

$$r_p = \frac{1}{3\pi} \frac{\Gamma \overline{E}_f}{\sigma_Y^2} \tag{14}$$

Using the average values measured from these experiments, we calculate plastic zone sizes of $r_p = 10$ nm for $\sim Li_{2.8}Si$ and $r_p = 40$ nm for $\sim Li_{0.7}Si$. The thicknesses at these concentrations are 900 and 450 nm, respectively. Thus, the plastic zone size is significantly smaller than the thickness of the film. It is also interesting to note that the cracks in lithiated silicon show features typical of brittle fracture (Figures 3 and 4). In particular, Figure 4 shows that the faces of the cracks are quite flat and perpendicular to the substrate. These images of brittle fracture may be contrasted with those of a ductile copper film on a polymer substrate.[48,49] In the latter case, large plastic deformation (e.g., local thinning of the film) is visible in the copper film, which resists the formation of brittle cracks. To reconcile the experimental observations of plastic flow during lithiation and brittleness during fracture in lithiated silicon, we surmise that, once the cracks begin propagating, they move fast relative to the mechanisms associated with plastic deformation in this system. That is, lithiated silicon is essentially elastic during the fracture process. Under this scenario, the analysis from linear fracture mechanics associated with eq 9 is valid.

It is also interesting to compare the values measured in this study to those found in literature for pure silicon. For instance, Ballarini et al. found the critical stress intensity factor for amorphous silicon to be $K_{IC} = 1 \text{ MPa·m}^{1/2}$.[50] This value was calculated assuming a value $E = 160$ GPa in their finite element simulations.[50] Using this value for the modulus gives a fracture energy of $\Gamma = K_{IC}^2/E = 6.3 \text{ J/m}^2$ for amorphous silicon. Likewise, values for fracture energy of single-crystal silicon are in the range of $3-9 \text{ J/m}^2$,[51] and comparable values can be found for bulk polycrystalline silicon.[52] Remarkably, the values for the fracture energy of pure silicon are quite comparable to the measured values for lithiated silicon at both small and large concentrations of lithium. Atomistic simulations have suggested that lithium insertion into silicon results in continuous breaking and reforming of Si−Si bonds, resulting in a decrease in strength and an increase in ductility.[53] As a result, one might expect that lithium insertion into silicon may drastically alter the fracture energy. The current experimental study suggests, however, that the fracture energy of lithiated silicon is not very different from pure silicon and does not vary substantially with lithium concentration. This finding is consistent with the SEM observations, which show characteristics of brittle fracture. If the fractured surfaces in lithiated silicon had shown features typical of ductile fracture, we would expect the fracture energy to be much larger than that of pure silicon. It appears that lithiated silicon has a peculiar ability to both flow plastically and fracture in a brittle manner. The mechanism causing this unique combination of properties warrants future investigation.

In conclusion, we have devised a novel method to electrochemically cycle multiple thin-film electrodes in parallel, while simultaneously measuring the film stress. We also monitored the morphological development of cracks by optical microscopy, which shows that cracks initially form and widen upon further delithiation, likely by a sliding mechanism as suggested in literature. This procedure allowed us to quantify the fracture energy of lithiated silicon. The fracture energy was determined to be $\Gamma = 8.5 \pm 4.3 \text{ J/m}^2$ at small concentrations of lithium ($\sim Li_{0.7}Si$) and to have bounds of $\Gamma = 5.4 \pm 2.2 \text{ J/m}^2$ and $\Gamma = 6.9 \pm 1.9 \text{ J/m}^2$ at large concentrations of lithium ($\sim Li_{2.8}Si$). These numbers are essential for mechanical models and can enable practical design of silicon electrodes that avoid mechanical degradation. The fracture energy does not vary significantly with lithium concentration and is not very different from pure silicon. We hope this work will provide guidance for practical design of silicon electrodes as well as motivate future modeling of lithiated silicon's unique ability to flow plastically but fracture in a brittle manner.

AUTHOR INFORMATION

Corresponding Author
*E-mail: vlassak@seas.harvard.edu.

Notes
The authors declare no competing financial interest.

REFERENCES

(1) Armand, M.; Tarascon, J. M. *Nature* **2008**, *451* (7179), 652−657.
(2) Service, R. F. *Science* **2011**, *332* (6037), 1494−1496.
(3) Ellis, B. L.; Lee, K. T.; Nazar, L. F. *Chem. Mater.* **2010**, *22* (3), 691−714.
(4) Marom, R.; Amalraj, S. F.; Leifer, N.; Jacob, D.; Aurbach, D. *J. Mater. Chem.* **2011**, *21* (27), 9938−9954.
(5) Zhang, W.-J. *J. Power Sources* **2011**, *196* (1), 13−24.
(6) Beaulieu, L. Y.; Eberman, K. W.; Turner, R. L.; Krause, L. J.; Dahn, J. R. *Electrochem. Solid State Lett.* **2001**, *4* (9), A137−A140.
(7) Deshpande, R.; Verbrugge, M.; Cheng, Y.-T.; Wang, J.; Liu, P. *J. Electrochem. Soc.* **2012**, *159* (10), A1730−A1738.
(8) Nadimpalli, S. P. V.; Sethuraman, V. A.; Dalavi, S.; Lucht, B.; Chon, M. J.; Shenoy, V. B.; Guduru, P. R. *J. Power Sources* **2012**, *215*, 145−151.
(9) Sethuraman, V. A.; Chon, M. J.; Shimshak, M.; Srinivasan, V.; Guduru, P. R. *J. Power Sources* **2010**, *195* (15), 5062−5066.
(10) Soni, S. K.; Sheldon, B. W.; Xiao, X.; Tokranov, A. *Scr. Mater.* **2011**, *64* (4), 307−310.
(11) Zhao, K.; Tritsaris, G. A.; Pharr, M.; Wang, W. L.; Okeke, O.; Suo, Z.; Vlassak, J. J.; Kaxiras, E. *Nano Lett.* **2012**, *12* (8), 4397−4403.

(12) Hertzberg, B.; Benson, J.; Yushin, G. *Electrochem. Commun.* **2011**, *13* (8), 818−821.

(13) Sethuraman, V. A.; Chon, M. J.; Shimshak, M.; Van Winkle, N.; Guduru, P. R. *Electrochem. Commun.* **2010**, *12* (11), 1614−1617.

(14) Kushima, A.; Huang, J. Y.; Li, J. *ACS Nano* **2012**, *6* (11), 9425−9432.

(15) Huggins, R. A.; Nix, W. D. *Ionics* **2000**, *6* (1−2), 57−63.

(16) Aifantis, K. E.; Hackney, S. A.; Dempsey, J. P. *J. Power Sources* **2007**, *165* (2), 874−879.

(17) Aifantis, K. E.; Hackney, S. A. *J. Power Sources* **2011**, *196* (4), 2122−2127.

(18) Zhao, K.; Pharr, M.; Vlassak, J. J.; Suo, Z. *J. Appl. Phys.* **2011**, *109*, 1.

(19) Zhao, K.; Pharr, M.; Wan, Q.; Wang, W. L.; Kaxiras, E.; Vlassak, J. J.; Suo, Z. *J. Electrochem. Soc.* **2012**, *159* (3), A238−A243.

(20) Xiao, X.; Liu, P.; Verbrugge, M. W.; Haftbaradaran, H.; Gao, H. *J. Power Sources* **2011**, *196* (3), 1409−1416.

(21) Haftbaradaran, H.; Xiao, X.; Verbrugge, M. W.; Gao, H. *J. Power Sources* **2012**, *206*, 357−366.

(22) Ryu, I.; Choi, J. W.; Cui, Y.; Nix, W. D. *J. Mech. Phys. Solids* **2011**, *59* (9), 1717−1730.

(23) Liu, X. H.; Zhong, L.; Huang, S.; Mao, S. X.; Zhu, T.; Huang, J. Y. *ACS Nano* **2012**, *6* (2), 1522−1531.

(24) Gao, Y. F.; Zhou, M. *J. Power Sources* **2013**, *230*, 176−193.

(25) Chan, C. K.; Peng, H.; Liu, G.; McIlwrath, K.; Zhang, X. F.; Huggins, R. A.; Cui, Y. *Nat. Nanotechnol.* **2008**, *3* (1), 31−35.

(26) Peng, K.; Jie, J.; Zhang, W.; Lee, S.-T. *Appl. Phys. Lett.* **2008**, *93*, 3.

(27) Baggetto, L.; Danilov, D.; Notten, P. H. L. *Adv. Mater.* **2011**, *23* (13), 1563−1566.

(28) Yao, Y.; McDowell, M. T.; Ryu, I.; Wu, H.; Liu, N.; Hu, L.; Nix, W. D.; Cui, Y. *Nano Lett.* **2011**, *11* (7), 2949−2954.

(29) Wu, H.; Chan, G.; Choi, J. W.; Ryu, I.; Yao, Y.; McDowell, M. T.; Lee, S. W.; Jackson, A.; Yang, Y.; Hu, L.; Cui, Y. *Nat. Nanotechnol.* **2012**, *7* (5), 309−314.

(30) Takamura, T.; Ohara, S.; Uehara, M.; Suzuki, J.; Sekine, K. *J. Power Sources* **2004**, *129* (1), 96−100.

(31) Yu, C.; Li, X.; Ma, T.; Rong, J.; Zhang, R.; Shaffer, J.; An, Y.; Liu, Q.; Wei, B.; Jiang, H. *Adv. Energy Mater.* **2012**, *2* (1), 68−73.

(32) Soni, S. K.; Sheldon, B. W.; Xiao, X.; Verbrugge, M. W.; Ahn, D.; Haftbaradaran, H.; Gao, H. *J. Electrochem. Soc.* **2012**, *159* (1), A38−A43.

(33) Shenoy, V. B.; Johari, P.; Qi, Y. *J. Power Sources* **2010**, *195* (19), 6825−6830.

(34) Stoney, G. G. *Proc. R. Soc. London, Ser. A* **1909**, *82* (553), 172−175.

(35) Nix, W. D. *Metall. Trans. A-Phys. Metall. Mater. Sci.* **1989**, *20* (11), 2217−2245.

(36) Obrovac, M. N.; Krause, L. J. *J. Electrochem. Soc.* **2007**, *154* (2), A103−A108.

(37) He, Y.; Yu, X.; Li, G.; Wang, R.; Li, H.; Wang, Y.; Gao, H.; Huang, X. *J. Power Sources* **2012**, *216*, 131−138.

(38) Beaulieu, L. Y.; Hatchard, T. D.; Bonakdarpour, A.; Fleischauer, M. D.; Dahn, J. R. *J. Electrochem. Soc.* **2003**, *150* (11), A1457−A1464.

(39) McArthur, M. A.; Trussler, S.; Dahn, J. R. *J. Electrochem. Soc.* **2012**, *159* (3), A198−A207.

(40) Chon, M. J.; Sethuraman, V. A.; McCormick, A.; Srinivasan, V.; Guduru, P. R. *Phys. Rev. Lett.* **2011**, *107* (4), 045503.

(41) Pharr, M.; Zhao, K.; Wang, X.; Suo, Z.; Vlassak, J. J. *Nano Lett.* **2012**, *12* (9), 5039−5047.

(42) McDowell, M. T.; Lee, S. W.; Harris, J. T.; Korgel, B. A.; Wang, C.; Nix, W. D.; Cui, Y. *Nano Lett.* **2013**, *13* (2), 758−764.

(43) Wang, J. W.; He, Y.; Fan, F.; Liu, X. H.; Xia, S.; Liu, Y.; Harris, C. T.; Li, H.; Huang, J. Y.; Mao, S. X.; Zhu, T. *Nano Lett.* **2013**, *13* (2), 709−715.

(44) Timoshenko, S. P.; Goodier, J. N. *Theory of Elasticity*, 3rd ed.; McGraw-Hill: New York, 1970.

(45) Nakamura, T.; Kamath, S. M. *Mech. Mater.* **1992**, *13* (1), 67−77.

(46) Beuth, J. L. *Int. J. Solids Struct.* **1992**, *29* (13), 1657−1675.

(47) Hutchinson, J. W. *J. Appl. Mechanics-Trans. ASME* **1983**, *50* (4B), 1042−1051.

(48) Lu, N.; Wang, X.; Suo, Z.; Vlassak, J. *Appl. Phys. Lett.* **2007**, *91*, 22.

(49) Lu, N.; Suo, Z.; Vlassak, J. J. *Acta Mater.* **2010**, *58* (5), 1679−1687.

(50) Ballarini, R.; Kahn, H.; Tayebi, N.; Heuer, A. H. Effects of Microstructure on the Strength and Fracture Toughness of Polysilicon: A Wafer Level Testing Approach. In *Mechanical Properties of Structural Films*; Muhlstein, C. L., Brown, S. B., Eds.; American Society for Testing and Materials: Orlando, FL, 2001; Vol. STP *1413*, pp 37−51.

(51) Ballarini, R.; Mullen, R. L.; Yin, Y.; Kahn, H.; Stemmer, S.; Heuer, A. H. *J. Mater. Res.* **1997**, *12* (4), 915−922.

(52) Chen, C. P.; Leipold, M. H.; Helmreich, D. *J. Am. Ceram. Soc.* **1982**, *65* (4), C49−C49.

(53) Zhao, K.; Wang, W. L.; Gregoire, J.; Pharr, M.; Suo, Z.; Vlassak, J. J.; Kaxiras, E. *Nano Lett.* **2011**, *11* (7), 2962−2967.